Frequency stabilization of self-sustained oscillations in a sideband-driven electromechanical resonator

B. Zhang,[1,2] Yingming Yan,[1,2] X. Dong,[1,2] M.I. Dykman,[3] and H.B. Chan[1,2,*]

[1] *Department of Physics, The Hong Kong University of Science and Technology, Clear Water Bay, Kowloon, Hong Kong, China*

[2] *William Mong Institute of Nano Science and Technology, The Hong Kong University of Science and Technology, Clear Water Bay, Kowloon, Hong Kong, China*

[3] *Department of Physics and Astronomy, Michigan State University, East Lansing, Michigan 48824, USA*

(Received 17 April 2024; accepted 6 September 2024; published 30 September 2024)

We present a method to stabilize the frequency of self-sustained vibrations in micromechanical and nanomechanical resonators. The method refers to a two-mode system with the vibrations at significantly different frequencies. The signal from one mode is used to control the other mode. In the experiment, self-sustained oscillations of micromechanical modes are excited by pumping at the blue-detuned sideband of the higher-frequency mode. Phase fluctuations of the two modes show near-perfect anticorrelation. They can be compensated in either of the modes by a stepwise change of the pump phase. The phase change of the controlled mode is proportional to the pump phase change, with the proportionality constant independent of the pump amplitude and frequency. This finding allows us to stabilize the phase of one mode against phase diffusion using the measured phase of the other mode. We demonstrate that phase fluctuations of either the high-frequency mode or the low-frequency mode can be significantly reduced. The results open new opportunities in generating stable vibrations in a broad frequency range via parametric down-conversion in nonlinear resonators.

DOI: 10.1103/PhysRevApplied.22.034072

I. INTRODUCTION

Self-sustained oscillations play a major role in diverse fields ranging from biological systems to lasers and clocks [1]. One of the most-important classes of systems that can display self-sustained oscillations is mechanical resonators. Examples include quartz oscillators that have long served as time references in ordinary clocks. In recent years, silicon micromechanical devices [2–5], because of their small size, have become viable alternatives to quartz oscillators in numerous applications, from telecommunications to smart watches. Self-oscillating micromechanical and nanomechanical devices are also used in high-precision measurements. Shifts in the vibration frequency enable measurement of force [6], charge [7], spin [8], and mass [9]. A well-known example is frequency-modulation atomic force microscopy [10]. The decrease of the size of mechanical resonators is generally expected to lead to an increase of fluctuations [11]. Suppressing fluctuations is a central problem in micromechanical and nanomechanical systems, and in particular in the systems that display self-sustained oscillations.

In micromechanical devices, the feedback needed to excite self-sustained oscillations is often implemented via an external circuit in which the signal generated by vibrations is phase-shifted and amplified to serve as the periodic drive [12–19]. Alternatively, the feedback mechanism can also be intrinsically built into the driven system, such as by photothermal effects [20–24] or other effects [25], or by measurement backaction [26].

Phase fluctuations in self-sustained oscillations are induced by different sources, from the thermal noise that arises from the coupling of the resonator to the environment to noise in various parts of the feedback circuit [27–29]. There have been many efforts to increase the phase stability of self-sustained oscillations in micromechanical and nanomechanical systems. In the linear regime, phase fluctuations induced by thermal noise decrease with the oscillation amplitude [30–32]. It is therefore beneficial to maximize the oscillation amplitude by operating the feedback circuit with a large external drive. However, if the oscillation amplitude is increased beyond the linear regime, the eigenfrequency of the resonator

*Contact author: hochan@ust.hk

becomes dependent on the amplitude. As a result, amplitude fluctuations are converted into frequency fluctuations. It was shown that, by designing the dependence of the eigenfrequency on amplitude to be nonmonotonic, phase noise can be minimized at the extremum where the eigenfrequency is locally independent of amplitude [18,33].

The nonlinear coupling to high-order modes has also been exploited to reduce phase noise. In these systems, the two modes are tuned into internal resonance, with the ratio of the eigenfreqeuncies of the modes being an integer. With energy exchanged between the modes, the phase fluctuations of the self-sustained oscillations of the low-frequency mode became much weaker [16,34].

Other approaches focus on mitigating the effects of noise generated by the feedback loop. For example, noise in the phase of the drive from the feedback loop can produce phase noise in the oscillations. This effect can be significantly reduced by driving a resonator into nonlinearity and picking an operation point where the vibration frequency is insensitive to the phase of the drive [12,35]. More recent work extended these concepts [15,36] and explored the possibility of surpassing the limit imposed by the thermomechanical noise [37]. Similar approaches were also used in minimizing the phase noise in self-sustained oscillations of two vibrational modes under a nondegenerate parametric drive [38].

An important distinction of self-sustained oscillations from forced oscillations is that the oscillation phase is arbitrary. In the presence of noise, fluctuations of the phase accumulate in time, resulting in phase diffusion [30,39–44]. Phase diffusion leads to decoherence, determining the spectral width of self-sustained oscillations. Minimizing phase diffusion is therefore paramount in applications of self-sustained oscillations ranging from high-sensitivity detection to high-stability frequency standards. To our knowledge, the possibility of significant reduction of phase diffusion in self-sustained oscillations has neither been explored theoretically nor demonstrated experimentally in micromechanical and nanomechanical oscillators.

In this paper, we present a scheme to stabilize the frequency of an important type of self-sustained oscillation induced by a drive with a frequency that is orders of magnitude different from the frequency of the vibrations of interest. We consider the vibrations induced by dynamical backaction in a sideband-driven micromechanical resonator with two nonlinearly coupled vibrational modes. The two modes have vastly different eigenfrequencies and decay rates, with the higher mode serving as an analogue of a photon cavity mode [43,45] in the context of cavity optomechanics [46,47]. A sufficiently strong pump applied at the blue-detuned sideband of the upper mode excites self-sustained vibrations [48–55] of both modes. In the stationary regime, the phase diffusion of the modes is anticorrelated. The sum of the phases remains essentially constant [43].

We show that the sum of the phases can be adjusted by the phase of the sideband pump and study the transient process in which such adjustment occurs when the pump phase is changed. For a step change of the pump phase, the phases of both modes settle to new values after a transient, the duration of which is determined by the smallest eigenvalue of the linearized equations of motion about the stable state. The phase change of each mode is proportional to the pump phase change, which is assumed to be small. Importantly, the two proportionality constants add up to unity. This finding, together with the phase anticorrelation of the two modes, allow us to stabilize the phase of one mode by measuring the phase of the other mode and then compensating for the phase diffusion by adjusting the phase of the pump. We demonstrate that phase fluctuations of either the high-frequency mode or the low-frequency mode can be significantly reduced. This results in a much-narrower spectral linewidth. Our scheme does not require a frequency reference near the mode to be stabilized, in contrast to direct feedback, which stabilizes a particular mode by measuring its phase. By exploiting the nonlinear coupling between two modes, the frequency reference could be orders of magnitude different from the eigenfrequency of the mode that is stabilized.

II. TWO-MODE ELECTROMECHANICAL SYSTEM

A. Excitation and detection of self-sustained vibrations

In our experiment, the micromechanical resonator consists of a square polysilicon plate ($100 \times 100 \times 3.5\ \mu m^3$) that is suspended by two beams of the same cross-section area ($1.3 \times 2\ \mu m^2$) but different lengths of 80 and 75 μm, respectively [Fig. 1(b)]. Fabrication was done with the surface micromachining process PolyMUMPs offered by MEMSCAP. The beams are covered by 30 nm of gold to reduce the electrical resistance. We use two vibrational modes in our experiment. For the low-frequency mode (mode 1), the plate undergoes translational motion normal to the substrate as the two beams are deformed [top in Fig. 1(c)]. The resonance frequency $\omega_1/2\pi$ is 47 030.7 Hz and the damping constant $\Gamma_1/2\pi$ is 0.48 Hz. The high-frequency mode (mode 2) is the lowest in-plane mode of the shorter beam [bottom in Fig. 1(c)], with resonant frequency $\omega_2/2\pi = 1\,867\,195.4$ Hz and damping constant $\Gamma_2/2\pi = 36.2$ Hz. Because of its significantly larger decay rate, in the presence of a weak external drive, mode 2 can play a role similar to optical or microwave modes in cavity optomechanics [46,47]. The change of the tension caused by the vibrations leads to a nonlinear coupling between the modes.

Forced vibrations of each mode can be excited by periodic electrostatic forces when small probe ac voltages are

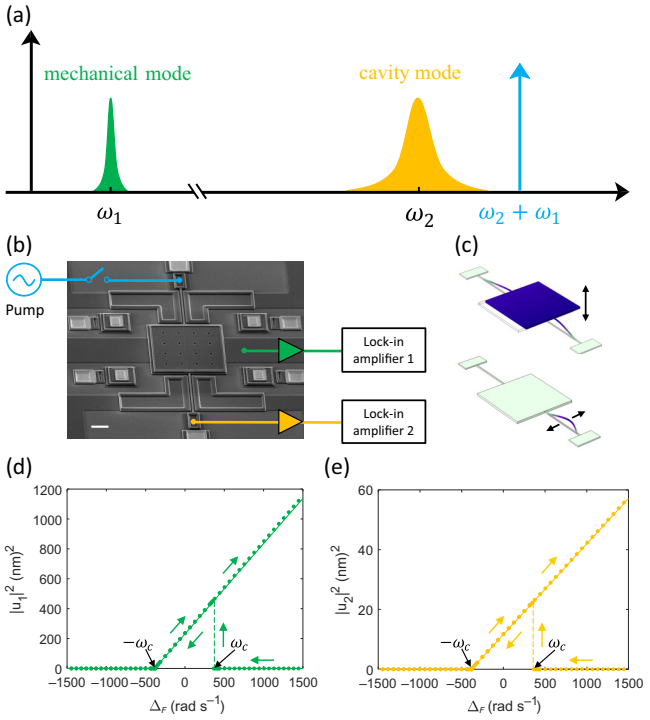

FIG. 1. (a) A sketch of the spectra of mode 1 (mechanical mode) and mode 2 (cavity mode). Energy of the pump that leads to self-sustained vibrations is supplied to the upper sideband of mode 2. (b) Scanning electron micrograph of the electromechanical resonator, including the measurement scheme. The white scale bar near the lower-left corner measures 30 μm. (c) Vibration profiles of mode 1 (top) and mode 2 (bottom). (d) Dependence of the square of the vibration amplitude of mode 1 on the detuning of the pump frequency from the upper sideband for mode 1 at pump-current amplitude of 189 μA. (e) Similar plot for mode 2.

applied to the electrodes nearby. For mode 2, vibrations can also be excited by the periodic Lorentz force when an alternating current is passed through the beams in a magnetic field perpendicular to the substrate. Motion of the plate in mode 1 is detected by measurement of the capacitance change between the plate and the underlying electrode. For mode 2, the overlap area of the beam with the electrodes is much smaller than for mode 1, resulting in greater detection noise for capacitive detection. To reduce the detection noise for mode 2, vibrations are detected instead by the change in the current due to the back electromotive force as the beam vibrates in the magnetic field. All measurements are conducted at a temperature of 4 K and a pressure of less than 10^{-5} Torr. These measurements allowed us to determine the values of the eigenfrequencies and decay rates of the modes.

To induce self-sustained oscillations, a periodic pump current at frequency ω_F close to the frequency sum $(\omega_1 + \omega_2)$ is applied through the beam to generate a Lorentz force as shown in Fig. 1(a). This force modulates the nonlinear coupling between the two modes. The equations of motion that describe the effect of such resonant modulation on the coupled-mode system are

$$\begin{aligned}
&\ddot{q}_1 + \omega_1^2 q_1 + 2\Gamma_1 \dot{q}_1 + \frac{\gamma_1}{m_1} q_1^3 + \frac{\gamma}{m_1} q_1 q_2^2 \\
&\quad = \frac{F}{m_1} q_2 \cos(\omega_F t + \theta_F), \\
&\ddot{q}_2 + \omega_2^2 q_2 + 2\Gamma_2 \dot{q}_2 + \frac{\gamma_2}{m_2} q_2^3 + \frac{\gamma}{m_2} q_2 q_1^2 \\
&\quad = \frac{F}{m_2} q_1 \cos(\omega_F t + \theta_F),
\end{aligned} \tag{1}$$

where q_1 and q_2 are the displacements of the plate and the beam center, respectively, m_1 and m_2 are the effective masses, and γ_1 and γ_2 are the Duffing nonlinearities of the two modes. The two modes are found to be dispersively coupled, where the vibration of one mechanical mode creates tension in the beams and in turn modifies the resonance frequency of the other mode (Appendix A). In Eq. (1), the dispersive coupling is represented by the terms with coupling constant γ that correspond to coupling energy $\frac{1}{2}\gamma q_1^2 q_2^2$. The parameter F gives the amplitude of the parametric sideband pumping, which is proportional to the amplitude of the applied pump current I_{pump}. The phase of the pump is θ_F. In the Hamiltonian of the coupled modes, the term corresponding to the pump is $-Fq_1q_2\cos(\omega_F t + \theta_F)$.

We assume that the pump frequency is close to $\omega_1 + \omega_2$, with the pump detuning $\Delta_F = \omega_F - (\omega_1 + \omega_2)$ much smaller than ω_F. By making the substitution $u_1 = \frac{1}{2}(q_1 - i\omega_1^{-1}\dot{q}_1)e^{-i\omega_1 t}$ and $u_2 = \frac{1}{2}(q_2 - i(\omega_F - \omega_1)^{-1}\dot{q}_2)\exp[-i(\omega_F - \omega_1)t]$ to convert q_1 and q_2 to slowly varying complex vibration amplitudes u_1 and u_2, and by applying the rotating-wave approximation, we obtain equations for u_1 and u_2:

$$\begin{aligned}
&\dot{u}_1 + \Gamma_1 u_1 - i\frac{3\gamma_{11}}{2\omega_1} u_1 |u_1|^2 - i\frac{\gamma_{12}}{\omega_1} u_1 |u_2|^2 = \frac{F_1 e^{i\theta_F}}{4i\omega_1} u_2^*, \\
&\dot{u}_2 + (\Gamma_2 + i\Delta_F) u_2 - i\frac{3\gamma_{22}}{2\omega_2} u_2 |u_2|^2 - i\frac{\gamma_{21}}{\omega_2} u_2 |u_1|^2 \\
&\quad = \frac{F_2 e^{i\theta_F}}{4i\omega_2} u_1^*,
\end{aligned} \tag{2}$$

where $\gamma_{11} = 1.91 \times 10^{22}$ rad^2 s^{-2} m^{-2}, $\gamma_{22} = 7.38 \times 10^{25}$ rad^2 s^{-2} m^{-2}, $\gamma_{12} = 8.41 \times 10^{22}$ rad^2 s^{-2} m^{-2} and $\gamma_{21} = 1.26 \times 10^{25}$ rad^2 s^{-2} m^{-2}. The parameters γ_{21}, γ_{22}, γ_{12} and γ_{21} contain contributions that account for the renormalization that arises from the nonlinear coupling of the modes [43]. The parameters F_1 and F_2 also account for the forces that are directly applied to the modes. We note that $F_1/F_2 = \gamma_{12}/\gamma_{21} = m_2/m_1$.

We first consider the case in which vibration amplitudes are small so that the terms involving γ_{11}, γ_{22},

γ_{12} and γ_{21} can be ignored. With $\Gamma_2 \gg \Gamma_1$, we apply the adiabatic approximation by setting $\dot{u}_2 = 0$ in the second equation in Eq. (2) because after a short transient, both $|\dot{u}_1/u_1|$ and $|\dot{u}_2/u_2|$ become much smaller than $\left(\Gamma_2{}^2 + \Delta_F^2\right)^{1/2}$. It follows from Eq. (2) that for $\Delta_F = 0$, $u_2 \approx (F_2 e^{i\theta_F}/4i\omega_2\Gamma_2)u_1^*$. Putting u_2 back into the first equation in Eq. (2) yields an effective damping constant of mode 1 that decreases with the pumping power as $\Gamma_1 - F_1F_2/16\omega_1\omega_2\Gamma_2$.

For sufficiently large pumping power, the effective damping becomes negative and self-sustained vibrations are excited. Both modes start oscillating at the same time, although with different amplitudes. Figures 1(d) and 1(e) shows these amplitudes for mode 1 and mode 2, respectively, as a function of Δ_F at a pump-current amplitude of 189 μA. The vibrations are excited when Δ_F is increased beyond a threshold value $-\omega_c$. This value can be found from the condition of the loss of stability of the stationary state $u_1 = u_2 = 0$, giving [43]

$$\begin{aligned} \omega_c &= (\Gamma_1 + \Gamma_2)\left[\Xi^2 - 1\right]^{\frac{1}{2}}, \\ \Xi &= (F_1F_2/16\omega_1\omega_2\Gamma_1\Gamma_2)^{1/2}. \end{aligned} \tag{3}$$

The vibration amplitude increases with Δ_F. At $\Delta_F = \omega_c$, the zero-amplitude state becomes stable again. Previous experiments [43] determined the dependence of ω_c on the pump power and studied the bistability and hysteretic behavior as Δ_F is varied.

B. Anticorrelated phase diffusion of the two modes

If the pump is not too strong, self-sustained vibrations of the two modes are sinusoidal, but their frequency deviates from ω_1 and ω_2. The deviation depends on the amplitude and frequency of the pump. To analyze the self-sustained vibrations, we write the variables u_1 and u_2 in the form of the amplitudes r_1, r_2 and phases ϕ_1, ϕ_2 of the vibrations and take into account that the vibrations in the rotating frame have frequency $\delta\omega$:

$$u_1 = r_1 e^{i\phi_1(t)} \exp(i\delta\omega t), \quad u_2 = r_2 e^{i\phi_2(t)} \exp(-i\delta\omega t). \tag{4}$$

In the steady state, r_1, r_2, ϕ_1, and ϕ_2 and are independent of time. In the laboratory frame, self-sustained oscillations in modes 1 and 2 occur at frequencies $\omega_{\text{self},1} = \omega_1 + \delta\omega$ and $\omega_{\text{self},2} = \omega_2 + \Delta_F - \delta\omega$, respectively.

It is convenient to write the equations of motion in the form

$$\begin{aligned} \dot{r}_i &= -\Gamma_i r_i + \frac{F_i}{4\omega_i}\frac{r_{3-i}}{r_i}\sin\Theta \quad (i = 1, 2), \\ \dot{\phi}_+ &= -\Delta_F + \sum_{i=1,2}\left[\frac{\gamma^{(+)}_{i\,3-i}}{\omega_i} r_{3-i}^2 - \frac{F_i}{4\omega_i}\frac{r_{3-i}}{r_i}\cos\Theta\right], \end{aligned} \tag{5}$$

and

$$\dot{\phi}_- = \Delta_F - 2\delta\omega - \sum_{i=1,2}(-1)^i\left[\frac{\gamma^{(-)}_{i\,3-i}}{\omega_i} r_{3-i}^2 - \frac{F_i}{4\omega_i}\frac{r_{3-i}}{r_i}\cos\Theta\right], \tag{6}$$

where

$$\phi_\pm = \phi_1 \pm \phi_2, \quad \Theta = \theta_F - \phi_+.$$

The explicit form of the coefficients $\gamma_{ij}^{(+)}$ and $\gamma_{ij}^{(-)}$ is given in Appendix B.

The stationary solution of Eqs. (5) and (6) gives the amplitudes $r_1^{(0)}, r_2^{(0)}$ and the phases $\phi_1^{(0)}, \phi_2^{(0)}$ of the self-sustained vibrations of the coupled modes, as well as the vibration frequency in the rotating frame $\delta\omega$. They are also listed in Appendix B. In particular, the total phase is expressed as

$$\phi_+^{(0)} = \theta_F - \Theta^{(0)}, \quad \Theta^{(0)} = \arcsin(1/\Xi), \tag{7}$$

where Ξ is defined in Eq. (3).

An important feature of Eq. (5) is that the evolution of the amplitudes r_1, r_2 and the total phase ϕ_+ is independent of the phase difference ϕ_-. At the same time, the evolution of ϕ_- depends on r_1, r_2, and ϕ_+ as well as the phase θ_F of the driving field but not on ϕ_- itself. It is this feature that enables efficient control of the mode phase.

While fluctuations in $\phi_1 + \phi_2$ do not accumulate, fluctuations in $\phi_1 - \phi_2$ do. Figure 2(a) shows the measured phase change $\delta\phi_1(t) = \phi_1(t) - \phi_1(0)$ and $\delta\phi_2(t) = \phi_2(t) - \phi_2(0)$ as a function of time as θ_F is kept constant. $\delta\phi_1(t)$ is almost perfectly anticorrelated with $\delta\phi_2(t)$, in agreement with Eq. (7). Previous work has demonstrated that the system undergoes phase diffusion, with the mean square phase change increasing with time [43]. Depending on the origin of the phase fluctuations, the diffusion was found to be either normal or anomalous. This phase diffusion leads to decoherence, determining the linewidth of the self-sustained vibrations. Figures 2(b) and 2(c) show the results given in Fig. 2(a) in frames rotating at the frequencies of self-sustained vibrations of the two modes, $\omega_{\text{self},1}$ and $\omega_{\text{self},2}$, respectively. The motion of the two modes in the tangential direction is not confined, but is correlated.

III. FREQUENCY STABILIZATION

With the phase anticorrelation of the two modes, one can measure the phase diffusion of one mode and infer the phase of the other mode without measuring it. This property enables the design of a scheme that uses the measured phase of one mode to stabilize the phase of the other mode, provided that there is a mechanism to alter the latter. We show below that either ϕ_1 or ϕ_2 can be stabilized by adjustment of the pump phase θ_F and use of the measured ϕ_2 or ϕ_1 as the error signal. An antecedent less-efficient

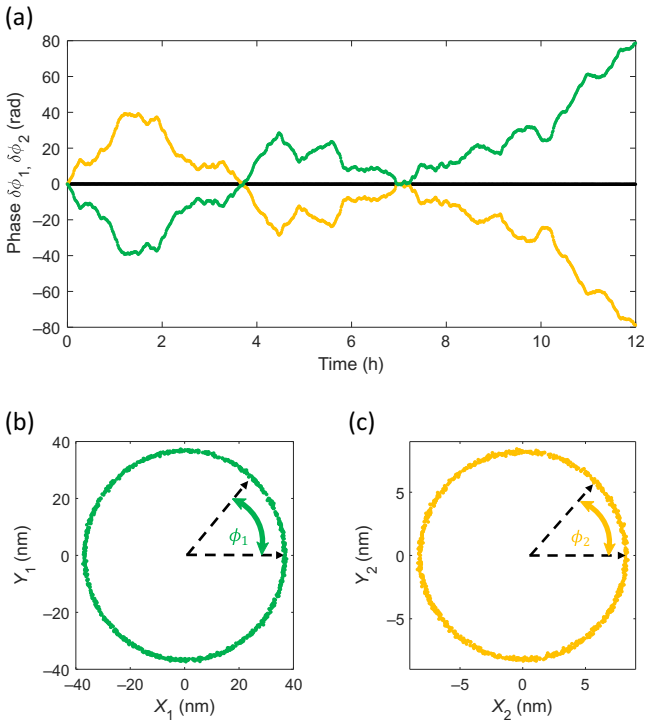

FIG. 2. (a) Change of the vibration phase $\delta\phi_1$ of mode 1 (green) and $\delta\phi_2$ of mode 2 (yellow), measured as a function of time. The black line represents the sum $\delta\phi_1 + \delta\phi_2$. The pump-current amplitude is 189 μA, corresponding to $F = 2.3$ mN m^{-1}, and frequency detuning Δ_F is 300 Hz. The same results are plotted in (b),(c) in the frames rotating at the frequencies $\omega_{\text{self},1}$ and $\omega_{\text{self},2}$ of the self-sustained vibrations of the two modes. The variables are $X_i = r_i \cos(\phi_i)$ and $Y_i = r_i \sin(\phi_i)$, $i = 1, 2$.

scheme was implemented in a previous experiment [43] to prove the concept for stabilizing mode 2. Here, we analyze in detail, quantitatively, the effect on the two modes when the pump phase θ_F is adjusted. Then we develop and optimize the stabilization scheme in our experimental system. Furthermore, we demonstrate that mode 1 can also be stabilized by measuring mode 2, despite requiring much larger changes in θ_F.

A. Effect of a change of pump phase

For short durations of phase accumulation, the noise-induced changes of the phases are small and can be compensated by small changes of θ_F. The effect can be analyzed by linearizing the equations in Eq. (5) about the stationary solution $r_1^{(0)}, r_2^{(0)}, \phi_+^{(0)}$. It is convenient to write the linearized equations for the increments:

$$x_1 = \zeta - \zeta^{(0)}, \quad x_2 = \theta_F - \phi_+ - \Theta^{(0)}, \quad x_3 = \frac{r_1 - r_1^{(0)}}{r_1^{(0)}},$$

where $\zeta \equiv r_2/r_1$. The corresponding equations have the form

$$\dot{x}_n = \Lambda_{nm} x_m \quad (n, m = 1, 2, 3), \tag{8}$$

where we imply summation over repeated indices. Appendix B gives the explicit form of the matrix $\hat{\Lambda}$. The initial conditions that correspond to incrementally changing θ_F by $\delta\theta_F$ at $t = 0$ are $x_1(0) = x_3(0) = 0$ and $x_2(0) = \delta\theta_F$.

For stable self-sustained vibrations described by Eq. (5) the eigenvalues λ_ν ($\nu = 1, 2, 3$) of the matrix $\hat{\Lambda}$ have negative real parts. Therefore $x_1(t)$, $x_2(t)$, and $x_3(t)$ become exponentially small for $t \gg t_r$, where the relaxation time $t_r = 1/\min|\text{Re}\,\lambda_\nu|$. This means that, over the relaxation time, ϕ_+ is incrementally changed by $\delta\theta_F$, i.e., $\delta\phi_+(t) \to \delta\theta_F$. For the rest of this paper, we use $\delta\phi_+(t), \delta\phi_-(t)$ and $\Delta\phi_+, \Delta\phi_-$ to denote, respectively, the transient and settled values of ϕ_+, ϕ_- changed from the initial values.

The eigenvalues λ_k can be found analytically near the bifurcation point $\Delta_F = -\omega_c$, where self-sustained vibrations emerge; see Appendix B. Here the eigenvalues λ_1 and λ_2 are complex conjugate, with the real part $-(\Gamma_1 + \Gamma_2)$. The eigenvalue λ_3 is real and small in absolute value, $\lambda_3 \propto \Delta_F + \omega_c$. Our numerical analysis shows that, for the parameters of our system, the eigenvalue λ_3 remains small in absolute value throughout the range we have explored; see Figs. 3(e) and 3(f). Therefore, the relaxation time $t_r = -1/\lambda_3$.

The incremental change $\delta\phi_-(t)$ of ϕ_- is described by the linearized form of Eq. (6), with $d\delta\phi_-/dt$ being a sum of the appropriately weighted $x_1(t)$, $x_2(t)$, and $x_3(t)$. Hence, $\delta\phi_-$(t) is given by the integrals over time of $x_1(t)$, $x_2(t)$, and $x_3(t)$. Since all variables $x_n(t)$ are proportional to $\delta\theta_F$ and all of them decay for $t \gg t_r$, we see that $\delta\phi_-(t) \to C\delta\theta_F$ for $t \gg t_r$, where C is determined by the parameters of the system; see Appendix C. Therefore incremental change of θ_F leads, after transient time comparable or larger than t_r, to

$$\Delta\phi_2 = g\delta\theta_F, \quad \Delta\phi_1 = (1 - g)\delta\theta_F, \quad g = (1 - C)/2. \tag{9}$$

1. Implementing phase increment of the driving field

The incremental change of the phase θ_F of the driving field is obtained by changing the driving frequency ω_F for a short time and then bringing it back to the original value. One scenario is where this time is on the order of $1/\omega_F$. Equations (2), (5), and (6) do not apply on this timescale. However, the change of the "slow" variables over time comparable to $1/\omega_F$ associated with the change of θ_F is small and can be disregarded. It applies to the case implemented in the experiment where θ_F is controlled by a digital function generator.

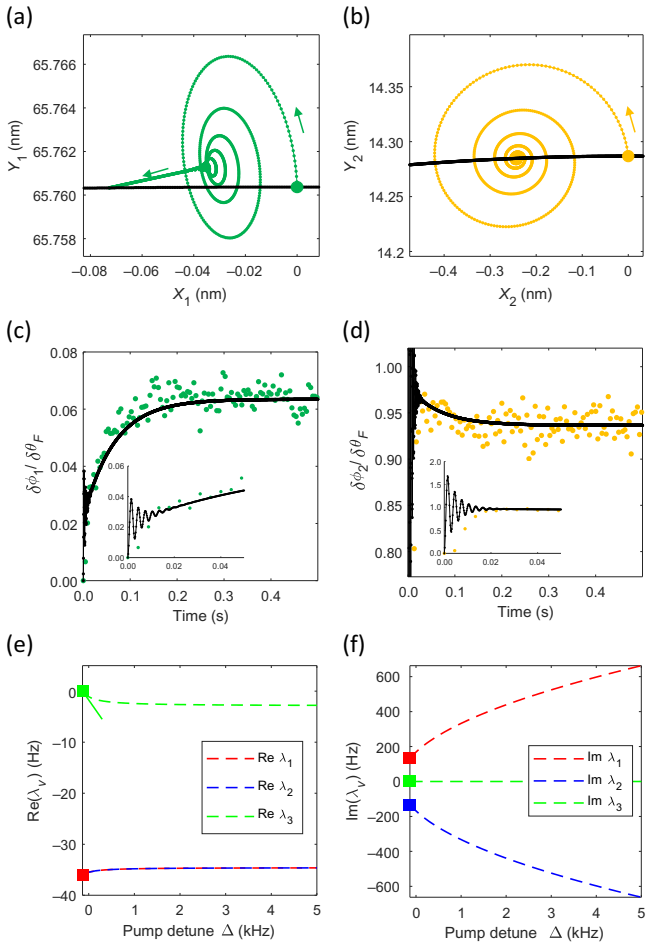

FIG. 3. (a) Numerical calculation of the dynamics of mode 1 in the frame rotating at frequency $\omega_{\text{self},1}$ in response to a sudden change of θ_F by 1°; $X_1 = r_1\cos\phi_1$ and $Y_1 = r_1\sin\phi_1$. The pump-current amplitude is 379 μA and frequency detuning Δ_F is 1000 Hz. Initially, X_1 is set to zero. The black line is part of the circles $X_1^2 + Y_1^2 = r_1^{(0)2}$. (b) Corresponding plot for mode 2. (c) Measured dependence of ϕ_1 on time (green circles). The solid line represents numerical simulations with no fitting parameters. Error bars are comparable to the spread of the data. The inset zooms in at shorter times. (d) Corresponding plot for mode 2. (e) Real parts of the eigenvalues for the matrix $\hat{\Lambda}$ in the linearized equation of motion plotted as a function of the pump detuning frequency. λ_1, λ_2, and λ_3 are plotted as dashed red, blue, and green lines, respectively. Near the supercritical Hopf bifurcation point, analytical expressions (Appendix B) give the solid green line for λ_3 and the red square for λ_1. (f) Similar plot for the imaginary parts of λ_1, λ_2, and λ_3.

Alternatively, the phase can be incrementally changed by changing the frequency ω_F over time much longer than $1/\omega_F$ but yet much shorter than $1/\max|\lambda_\nu|$. The dynamics in this case is described by Eqs. (5) and (6). It can be modeled by assuming that Δ_F is changed by $\delta\theta_F\delta(t)$. As seen from Eq. (5), this is equivalent to the initial condition $x_2(t\to+0) = \delta\theta_F$. However, ϕ_- is also incrementally changed by $\delta\theta_F$.

Yet another way of changing the phases is to apply a pulse of $\Delta_F(t)$ with $\Delta_F(t)$ varying slowly on the scale t_r. The change of the variables x_n, ϕ_- can be then described in the adiabatic approximation. This leads to simple explicit expressions for this change; see Appendix C. Unexpectedly, the result allows one also to express C in Eq. (9) in a simple explicit form, which does not require diagonalization of the matrix $\hat{\Lambda}$.

We note that the frequency of self-sustained vibrations can be obtained in an alternative way. One could omit $\delta\omega$ in defining the variables r_1, r_2, ϕ_1, and ϕ_2 in Eq. (4). This omission will not affect the equations of motion (5) for r_1, r_2, ϕ_+; that is, they will have the same form. The stationary solution of these equations gives $r_1^{(0)}, r_2^{(0)}, \phi_+^{(0)}$, and this solution is stable for $\Delta_F + \omega_c > 0$, since Re $\lambda_\nu < 0$ ($\nu = 1,2,3$). On the other hand, Eq. (6) will have as a solution $\dot{\phi}_-$ equals a constant. The value of this constant is $-2\delta\omega$; see Eq. (B3). In the stationary state, the complex amplitudes $u_1(t)$ and $u_2(t)$ oscillate at frequencies $\delta\omega$ and $-\delta\omega$, respectively.

2. Measurement of the effect of a step change of the pump phase

Figures 3(a) and 3(b) show that both the amplitude and the phase are perturbed by a step change in the pump phase, for mode 1 and mode 2, respectively. Details of the calculations of the transient are described in Appendix C. There are two stages in the transient response. The system first relaxes quickly following the spirals, the decay rate and frequency of which are determined by the real and imaginary parts of the eigenvalues λ_1 and λ_2, respectively. As described earlier in this section, λ_1 and λ_2 are complex conjugates of each other. The second part of the transient is marked by the arrow pointing to the left in Fig. 3(a) for mode 1. On this part of the phase trajectory, the system approaches the new stable state at a much slower rate given by λ_3 and the fast variables follow the slow variable adiabatically. For mode 2, the second stage of relaxation occurs over a much smaller range in Fig. 3(b) and is difficult to identify.

After the transient, the amplitudes r_1, r_2 of the self-sustained vibrations go back to the original values. The phases change by $\Delta\phi_1, \Delta\phi_2$ as given by Eq. (9), assuming that phase diffusion induced by noise is negligible. In particular, $\Delta\phi_1 + \Delta\phi_2$ equals $\delta\theta_F$ after the transient, according to Eq. (7).

As described later, the algorithms to stabilize the phases ϕ_1, ϕ_2 requires one knowing the ratio $g = \Delta\phi_2/\delta\theta_F$, which denotes the fraction of the change in the pump phase taken up by mode 2. The fraction of the change in the pump phase taken up by mode 1 is $1 - g = \Delta\phi_1/\delta\theta_F$. The value of g is determined by Eqs. (9) and (C8). We find that g depends only on system parameters, including the damping

constants, effective masses, and nonlinear coupling coefficients, but is independent of the pump detuning frequency and amplitude (Appendix C). For our system parameters, $g = 0.94$. A change in the phase of the pump therefore affects both mode 1 and mode 2. However, the effect on mode 2 far exceeds that on mode 1.

We measure the response of the two modes for a duration of 0.5 s after θ_F is abruptly changed by 1°. θ_F is controlled by a digital function generator. It changes over a timescale of approximately ω_F^{-1}, as indicated above, much shorter than $|\lambda_1^{-1}|$, $|\lambda_2^{-1}|$, and $|\lambda_3^{-1}|$. The measurement is performed 7200 times and the averaged phase changes scaled by the pump step, $\delta\phi_1(t)/\delta\theta_F, \delta\phi_2(t)/\delta\theta_F$, are plotted in Figs. 3(c) and 3(d), respectively, as green and yellow dots at detuning $\Delta_F = 1000$ Hz and an amplitude of 379 μA of the pump current, which corresponds to $F = 4.5$ mN m^{-1}. Averaging is necessary to resolve the change from detection noise and the noise introduced by phase diffusion. The agreement between measurement and theory is good on the slow-relaxation timescale, which in our case was 0.3 s, with no fitting parameters. However, it is not feasible for us to measure the fast relaxation represented by the solid lines in the insets, as it requires a much larger bandwidth for the lock-in amplifier, which significantly increases the detection noise.

Apart from the transient response, the measured values of $\Delta\phi_1, \Delta\phi_2$ in the steady state also agree with the calculations: mode 2 accounts for most of the phase change (94%) in response to $\delta\theta_F$, while the remaining 6% occurs in mode 1. As plotted in Fig. 3(e), the dashed green line represents the eigenvalue λ_3 that determines the rate of the slow relaxation. $|\lambda_3|$ first increases with increasing pump detuning, then remains largely constant when pump detuning exceeds 2 kHz. The red and blue lines plot the real parts of λ_1 and λ_2, which determine the rate of the fast relaxation. Figure 3(f) shows the imaginary parts of eigenvalues λ_1 and λ_2, which are associated with the frequency of spiraling in Figs. 3(a) and 3(b). The relaxation rates change for other pump detuning values.

The ability to control the phase of the modes by adjusting $\delta\theta_F$, together with the near-perfect anticorrelation in the phase diffusion of modes 1 and 2, allows us to implement a scheme to stabilize the phase of mode 2 (mode 1) over timescales longer than $|\lambda_3^{-1}|$, by measuring the phase of mode 1 (mode 2), which vibrates at a different frequency.

IV. FREQUENCY STABILIZATION

A. Stabilization algorithm

We first discuss how the phase of mode 2 can be stabilized by measuring mode 1. Figure 4(a) shows the stabilization algorithm. The procedure starts at time $t = 0$, at which we define $\phi_1(t=0) = \phi_2(t=0) = \theta_F(t=0) = 0$ for convenience. In each cycle, ϕ_1 is measured. Then the

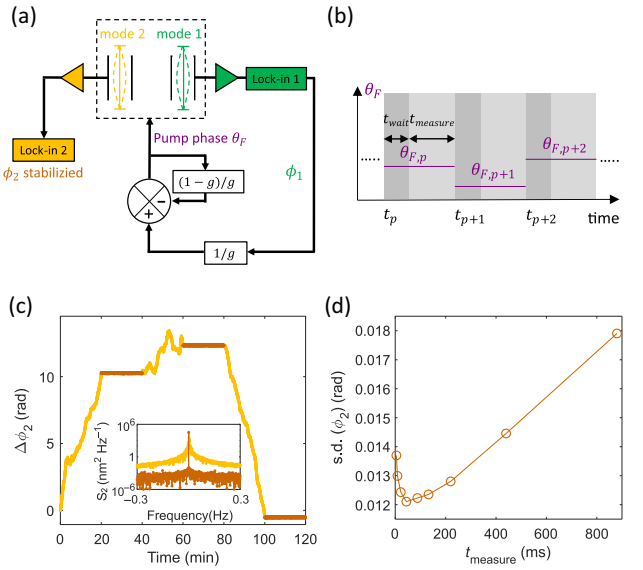

FIG. 4. (a) Algorithm for stabilizing ϕ_2 by measuring ϕ_1 and adjusting θ_F. (b) The duration of one cycle equals $t_{\text{wait}} + t_{\text{measure}}$. The pth cycle lasts from time t_p to time t_{p+1}. θ_F is changed only at the beginning of each cycle. (c) ϕ_2 is measured as a function of time when the stabilization routine is turned off for 20 min (yellow) and on for 20 min (brown). The pump-current amplitude is 189 μA and frequency detuning is 300 Hz. The inset shows the spectra S_2 of the self-sustained vibrations of mode 2 when the stabilization algorithm in (b) is implemented. The spectral width is significantly reduced with stabilization turned on. (d) Dependence of the standard deviation of ϕ_2 on t_{measure} at fixed t_{wait} of 300 ms.

pump phase θ_F is adjusted accordingly in the subsequent cycle to bring ϕ_2 close to zero. The duration of each cycle Δt is chosen to exceed the relaxation time $|\lambda_3^{-1}|$. The pth cycle lies in the time interval $t_p < t < t_{p+1}$, where $t_p = p\Delta t$ and p is a positive integer. θ_F is modified only at the beginning of a cycle at t_p, to a value $\theta_{F,p}$ determined by the algorithm described below. It remains fixed at other times.

Let $\phi_{1,\text{diffuse}}(t)$ and $\phi_{2,\text{diffuse}}(t)$ represent the phase change of mode 1 and mode 2, respectively, that arises solely due to phase diffusion. In the pth cycle, after the system has settled in response to changes in θ_F that occurred at t_p, the phases of the two modes are given by

$$\begin{aligned} \phi_1(t) &= \phi_{1,\text{diffuse}}(t) + (1-g)\,\theta_{F,p}, \\ \phi_2(t) &= \phi_{2,\text{diffuse}}(t) + g\theta_{F,p}. \end{aligned} \tag{10}$$

Here, the second terms on the right-hand side account for the effect of the change in pump phase $\theta_{F,p}$, which is split between modes 1 and 2 according to a fixed ratio g that was discussed in Sec. III A. Our goal is to choose $\theta_{F,p+1}$ in the next cycle to maintain $\phi_2(t)$ close to zero. As discussed in Sec. II B, there is near-perfect anticorrelation in the phase diffusion of modes 1 and 2 for fixed $\theta_{F,p}$. In other

words, $\phi_{2,\mathrm{diffuse}}(t)$ can be inferred by measuring mode 1, without measuring mode 2 itself. Rearrangement of the first equation in Eq. (10) yields

$$\phi_{2,\mathrm{diffuse}}(t) = -\phi_{1,\mathrm{diffuse}}(t) = (1-g)\,\theta_{F,p} - \phi_1(t). \quad (11)$$

The measurement of $\phi_1(t)$, however, takes a finite amount of time of data averaging to reduce the noise introduced by the detection circuit. As shown in Fig. 4(b), at the beginning of each cycle, the system is first allowed to settle in response to the change in θ_F. Then the measurement of ϕ_1 is performed over time t_{measure} to yield an averaged value $\tilde{\phi}_{1,p}$. The pump phase $\theta_{F,p+1}$ for the next cycle is chosen by replacing $\phi_1(t)$ in Eq. (11) by $\tilde{\phi}_{1,p}$ and then substituting $\phi_{2,\mathrm{diffuse}}(t)$ into the second equation in Eq. (10) with $\phi_2(t)$ set to zero and p replaced by $p+1$, yielding

$$\theta_{F,p+1} = \frac{1}{g}[\tilde{\phi}_{1,p} - (1-g)\,\theta_{F,p}]. \quad (12)$$

For stabilization of the phase of mode 2, the pump phase for the $(p+1)$th cycle is thus determined by both the measured phase of mode 1 and the pump phase chosen for the pth cycle.

To keep $\phi_2(t)$ small, we choose the time interval Δt to be short. Consequently, the increment $\theta_{F,p+1} - \theta_{F,p} = (\tilde{\phi}_{1,p} - \theta_{F,p})/g$ is small. To understand the evolution of the increments of $\theta_{F,p}$ we assume that immediately before the $(p+1)$th correction, i.e., for $t = t_{p+1} - \delta$ with small $\delta > 0$, there are small deviations of ϕ_2 from the target value of zero, so that $\phi_2(t) = \varepsilon_p$, with $|\varepsilon_p| \ll 1$ being a random number. If we set $\phi_1(t_{p+1} - \delta) = \tilde{\phi}_{1,p}$, i.e., if we disregard the change of $\phi_1(t)$ over time t_{measure} and ignore the uncertainty in measuring ϕ_1, we have from Eq. (10) $\tilde{\phi}_{1,p} = \theta_{F,p} - \varepsilon_p$. The increment in pump phase is then given by

$$\theta_{F,p+1} - \theta_{F,p} = -\varepsilon_p/g. \quad (13)$$

With $g \sim 0.94$ in our experiment, $|\theta_{F,p+1} - \theta_{F,p}|$ is indeed small. In a way one can think of this equation as a discrete analogue of a Langevin equation. The values of ε_p are determined by the imprecision of the measurements of the phase and of the control, and it is reasonable to assume that ε_p with different p are uncorrelated. Then $\langle \theta_{F,p}^2 \rangle$ increases with the number of cycles as $p\,\langle \varepsilon_p^2 \rangle / g^2$.

As discussed in Sec. III A, a step change in θ_F leads to changes in both ϕ_1 and ϕ_2. Therefore, the phase of mode 1 can also be stabilized by measuring the phase of mode 2 and adjusting θ_F to compensate for the phase diffusion. However, since $\Delta\phi_1/\delta\theta_F = 1 - g \ll 1$, the required $\delta\theta_F$ is much larger than what is needed for stabilization of mode 2, for comparable phase diffusion. The algorithm for stabilizing mode 1 is shown in Fig. 5(a). It is similar to that for stabilizing mode 2, except that mode 2 is measured

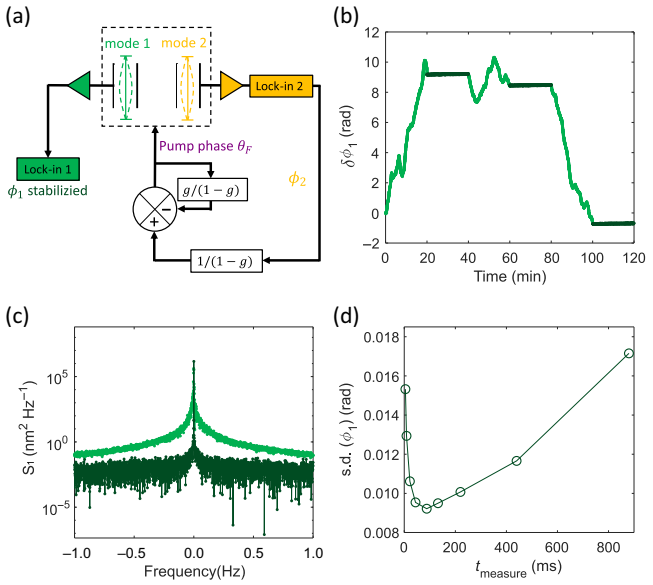

FIG. 5. (a) Algorithm for stabilizing ϕ_1 by measuring ϕ_2 and adjusting θ_F. (b) ϕ_1 is measured as a function of time when the stabilization routine is turned off (green) and on (dark green). The pump-current amplitude is 189 μA and frequency detuning is 300 Hz. (c) The spectra S_1 of the self-sustained vibrations of mode 1 with and without stabilization. (d) Dependence of the standard deviation of ϕ_1 on t_{measure} at fixed t_{wait} of 300 ms.

instead and the factor g in Eqs. (12) and (13) is replaced with $1-g$:

$$\theta_{F,p+1} = \frac{1}{1-g}\left[\tilde{\phi}_{2,p} - g\theta_{F,p}\right], \quad (14)$$

$$\theta_{F,p+1} - \theta_{F,p} = -\varepsilon_p/(1-g), \quad (15)$$

where $\tilde{\phi}_{2,p}$ is the measured value of ϕ_2 at the end of the pth cycle. In Eq. (14), $\theta_{F,p}$ is multiplied by approximately 16. It is therefore essential to take into account the effect of the pump phase change on mode 2 for the stabilization scheme to work properly for mode 1. By comparing Eq. (15) with Eq. (13), we find that the increment in pump phase required for stabilizing mode 1 is much larger than that required for stabilizing mode 2, which is consistent with the fact that mode 1 only takes up a small fraction (approximately 6%) of a step change of the pump phase.

B. Implementation

We demonstrate stabilization of the vibration frequencies for a pumping current of 189 μA at detuning frequency $\Delta_F = 300$ Hz. Figure 4(c) shows how the phase of mode 2 is stabilized by adjusting θ_F on the basis of measurement of ϕ_1. ϕ_1 and ϕ_2 are measured with two lock-in amplifiers referenced to $\omega_{\mathrm{self},1}$ and $\omega_{\mathrm{self},2}$, respectively, with a time constant of 1 ms. Measurements are recorded every 4.4 ms. t_{wait} is chosen as 300 ms, which exceeds the settling

time in response to a step change in θ_F. t_{measure} is chosen as 44 ms. Without stabilization, ϕ_2 undergoes diffusion (yellow). The phase fluctuations determine the width of the spectral peak in the inset in Fig. 4(b). When the stabilization is turned on (brown), fluctuations in ϕ_2 on timescales $\gtrsim$1 s are significantly reduced. Spectral components close to $\omega_{\text{self},2}$ are suppressed to levels given by the noise in the detection circuit. For example, the single-sideband phase noise at an offset of 0.1 Hz is reduced by 29 dB with phase stabilization turned on.

We optimize the stabilization algorithm with respect to t_{measure}. Figure 4(d) shows the standard deviation σ_{ϕ_2}, i.e., the root-mean-square value of ϕ_2, measured as a function of t_{measure} for constant t_{wait} of 300 ms. As t_{measure} increases from the minimum value of 4.4 ms, σ_{ϕ_2} initially decreases because a greater t_{measure} reduces the uncertainty introduced by the detection noise in measuring ϕ_1 that is used to determine θ_F in the subsequent stabilization cycle. However, with further increase of t_{measure}, σ_{ϕ_2} increases. This rise occurs because the value $\tilde{\phi}_{1p}$, which is used to determine the control signal $\theta_{F,p+1}$ and is obtained by averaging $\phi_1(t)$ over time t_{measure}, is increasingly different from the actual value $\phi_1(t_{p+1})$ required for efficient control. This difference is due to the phase diffusion. The optimal t_{measure} depends on the detection noise and both the intensity and the correlation time of the noise that leads to the phase diffusion. It should be shorter than this correlation time. We find that in our experiment, when $t_{\text{measure}} > 200$ ms, phase diffusion becomes the dominant effect and leads to the rise in σ_{ϕ_2}. The optimal measured σ_{ϕ_2} is approximately 12 mrad, attained at $t_{\text{measure}} \sim 44$ ms.

Figure 5(b) shows the stabilization of the phase of mode 1 by adjusting θ_F on the basis of measurement of ϕ_2 using Eq. (14). The spectral width of mode 1 is also reduced significantly, as shown in Fig. 5(c). In Fig. 5(d), the optimal value of σ_{ϕ_1} is approximately 9.5 mrad, attained at $t_{\text{measure}} \sim 88$ ms. A larger t_{measure} is needed than in the case of stabilizing mode 2, consistent with the fact that the uncertainty in detecting ϕ_2 is larger than that of detecting ϕ_1 in our experiment.

V. DISCUSSION AND OUTLOOK

Efficient stabilization of the phase of one mode relies on accurate determination of the phase of the other mode. The effect of the noise introduced by the detection circuits on the latter can be reduced by increasing the amplitude of the self-sustained oscillations. One way to achieve high amplitudes for the self-sustained vibrations is to choose large pump detuning, as shown in Figs. 1(d) and 1(e). For parameters chosen in our experiment, we have not encountered problems with stabilizing mode 2. However, in stabilizing mode 1, the change in the pump phase required to compensate for the phase diffusion is much larger than the phase diffusion itself [Eq. (14)]. We find that occasionally pump phase changes of up to 20° are required in our experiment. Such a large change of the pump phase could perturb the system such that it switches to the zero-amplitude state if the pump detuning exceeds ω_c. To avoid this problem, it is necessary to limit the pump detuning frequency to values smaller than ω_c so that the zero-amplitude state does not become stable.

In the stabilization algorithm, the pump phase is adjusted once per cycle. As a result, phase diffusion on timescales shorter than the cycle period are not compensated for. The duration of one stabilization cycle Δt is the sum of t_{wait} and t_{measure}. In our experiment, t_{wait} is chosen to barely exceed the settling time of the system in response to a step change in the pump phase. As shown in Figs. 4(d) and 5(d), the value of t_{measure} that gives optimal σ_{ϕ_1} or σ_{ϕ_2} is much shorter than t_{wait}. Further improvements to extend the stabilization to shorter timescales would rely on tuning of the system parameters (Appendix D) or the design of new resonators to achieve a shorter settling time.

To summarize, we present an algorithm to stabilize the frequency of self-sustained oscillations that are induced by dynamical backaction in a sideband-driven micromechanical resonator. It is based on adjustment of the phase of the pump to compensate for phase diffusion. When the system undergoes phase diffusion in the presence of weak noise, the phases of modes 1 and 2 add up to a constant (within our detection limit) that can be adjusted by the phase of the sideband pump. For a step change of the pump phase, the phases of both modes settle to new values after a transient. The duration of the transient is determined by the smallest real part of the eigenvalues of the linearized equations of motion about the vibrational state. If the pump change is small, the phase change of each mode is proportional to the pump phase change. The two proportionality constants add up to 1. This finding, together with the phase anticorrelation of the two modes, allow us to stabilize the phase of one mode by measuring the phase of the other mode and then compensating for the phase diffusion by adjusting the phase of the pump. We demonstrate that phase fluctuations of either the high-frequency mode or the low-frequency mode can be significantly reduced, resulting in a much-narrower spectral linewidth. The control algorithm requires knowledge of the phase shifts of the modes in response to a shift in the pump phase. After the transient, the proportionality constant between the mode phase shifts and the pump phase shift is independent of the parameters of the pump. It is fully determined by the parameters of the resonators.

The main advantage of our scheme is the significant reduction of phase diffusion of the self-sustained oscillations due to low-frequency noise, which plays an important role in nanomechanics and micromechanics. While other methods, such as those using nonlinear mode coupling [16,34] or nonmonotonic amplitude-frequency dependence [18,33], increase the frequency stability with respect to

noise with frequencies close to the resonator eigenfrequency, they do not protect against low-frequency noise. Therefore, phase fluctuations, albeit reduced, still accumulate in time and lead to phase diffusion. Our scheme, on the other hand, allows compensation of the slow phase diffusion of one mode by measuring the other mode and adjusting the pump phase. Phase diffusion is practically eliminated over timescales greater than Δt, limited only by the detection uncertainly of the other mode.

Future efforts will explore the possibility of combining our scheme with other approaches that increase the phase stability with respect to noise at comparatively high frequencies. For example, by designing one mode to have nonmonotonic amplitude-frequency dependence [18,33], one may be able to increase the oscillation amplitude for more-accurate determination of the phase that is subsequently used for choosing the phase of the pump for stabilizing the other mode.

The results open new opportunities in generating stable mechanical vibrations via parametric down-conversion in nonlinear micromechanical resonators, with controlled amplitude and phase. We reiterate that our scheme is distinct from direct feedback, which involves stabilizing a particular mode by measuring its phase, because a frequency reference near this mode is not required. As long as a frequency reference is available to determine the phase diffusion of one of the modes, the phase of the other mode can be stabilized even if its eigenfrequency is orders of magnitude different from that of the former. In principle, one can design resonators with the upper mode reaching microwave frequencies, in which the construction of signal sources with low phase noise and small long-term drift requires complex circuitry. The analysis also can be extended to mechanical resonators coupled to optical or microwave cavities [46,47].

By choosing the frequency and amplitude of the pump, the frequency of the self-sustained oscillations of the mode that is stabilized is readily tunable and therefore can serve as a frequency reference to characterize the frequency stability of other oscillators at different frequencies. Apart from potential applications in timekeeping, the stabilization scheme could also be used in sensing. With the oscillation phase of one of the modes stabilized, changes in its eigenfrequency lead to variations in the oscillation amplitude. Specific applications to sensing is an interesting topic that warrants further analysis.

ACKNOWLEDGMENTS

This work was supported by the Research Grants Council of Hong Kong SAR, China (Project No. 16304219). M.I.D. acknowledges partial support from the U.S. Defense Advanced Research Projects Agency (Grant No. HR0011-23-2-004) and from the Moore Foundation (Grant No. 12214).

APPENDIX A: DISPERSIVE COUPLING BETWEEN MODES 1 AND 2

Modes 1 and 2 in the resonator are dispersively coupled, with interaction energy of the form $\frac{1}{2}\gamma q_1^2 q_2^2$. Figure 6 shows that the decrease in the resonant frequency of one mode is proportional to the square of the vibration amplitude of the other mode. In this measurement, the sideband pumping is removed. Instead, ac voltages at frequencies close to ω_1 and ω_2 are applied to the side gates of modes 1 and 2, respectively, to generate periodic electrostatic forces to excite forced vibrations at amplitudes A_1 and A_2. From the slopes of the linear fits, γ is determined to be 6.41×10^{12} kg rad^2 s^{-2} m^{-2}.

APPENDIX B: EIGENVALUES FOR THE LINEARIZED EQUATIONS OF MOTION NEAR THE SUPERCRITICAL HOPF BIFURCATION POINT

The nonlinearity parameters in the equation for the phases of self-sustained vibrations [Eq. (5)] have the form

$$\gamma_{ij}^{(\pm)} = \gamma_{ij} \pm \frac{3\gamma_{jj}\omega_i}{2\omega_j} \quad (i,j = 1,2; i \neq j). \tag{B1}$$

By setting $\dot{r}_1 = \dot{r}_2 = \dot{\phi}_\pm = 0$ in Eqs. (5), we obtain the ratio of the stationary amplitudes $r_1^{(0)}, r_2^{(0)}$ and the phase $\phi_+^{(0)} \equiv \phi_1^{(0)} + \phi_2^{(0)}$ (see Ref. [43]):

$$\begin{aligned} &\sin\Theta^{(0)} = 1/\Xi, \quad \Theta^{(0)} = \theta_F - \phi_+^{(0)}, \\ &\zeta^{(0)} \equiv r_2^{(0)}/r_1^{(0)} = (\Gamma_1 F_2 \omega_1 / \Gamma_2 F_1 \omega_2)^{1/2}, \end{aligned} \tag{B2}$$

where Ξ is given by Eq. (3).

The vibration frequency in the rotating frame $\delta\omega$ and the squared radius of the vibrations of mode 1 are given by the

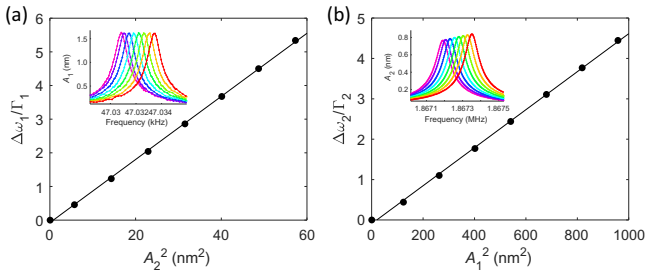

FIG. 6. (a) Scaled shifts of the frequency of mode 1 versus the square of the amplitude A_2 of forced vibrations in mode 2. The line is a linear fit through the origin. The inset shows spectra of mode 1 under a periodic electrostatic force. Each resonance peak corresponds to a data point in the main panel. (b) A similar plot for mode 2.

expressions

$$\delta\omega = \left(\frac{\gamma_{12}}{\omega_1}\zeta^{(0)2} + \frac{3\gamma_{11}}{2\omega_1}\right) r_1^{(0)2} - \Gamma_1\left(\Xi^2-1\right)^{\frac{1}{2}},$$
$$r_1^{(0)2} = \frac{\Gamma_2\omega_2 F_1}{\gamma_{21}^{(+)}\Gamma_2 F_1 + \gamma_{12}^{(+)}\Gamma_1 F_2}\left(\Delta_F + \omega_c\right), \tag{B3}$$

where the critical detuning ω_c is given by Eq. (3), $\omega_c = (\Gamma_1+\Gamma_2)(\Xi^2-1)^{1/2}$.

The linearized equations of motion [Eq. (8)] for the increments

$$x_1 = \delta\zeta, \quad x_2 = \theta_F - \delta\phi_+ - \Theta^{(0)}, \quad x_3 = \delta r_1/r_1^{(0)}$$

of the dynamical variables $\zeta = r_2/r_1, \phi_+ = \phi_1+\phi_2$, and r_1 follow from Eq. (5). We write them in a vector form for the vector $\mathbf{x}$ with components x_1, x_2, x_3. We emphasize that the unknown quantity is $\delta\phi_+$. It is a dynamical variable, whereas θ_F is the control parameter. Therefore, $\dot{x}_2 \equiv -d\delta\phi_+/dt$. The equations read

$$\begin{aligned}
&\dot{\mathbf{x}} = \hat{\Lambda}\mathbf{x}, \quad \Lambda_{11} = -\left(\Gamma_1+\Gamma_2\right), \quad \Lambda_{12} = \left(\Gamma_2-\Gamma_1\right)\zeta^{(0)}\left(\Xi^2-1\right)^{1/2}, \quad \Lambda_{13} = 0,\\
&\Lambda_{21} = -\left(\Gamma_2-\Gamma_1\right)\left(\Xi^2-1\right)^{1/2}/\zeta^{(0)} - \left(2\gamma_{12}^{+}/\omega_1\right) r_1^{(0)2}\zeta^{(0)},\\
&\Lambda_{22} = -(\Gamma_1+\Gamma_2), \quad \Lambda_{23} = -2[\left(\gamma_{12}^{+}/\omega_1\right)\zeta^{(0)2} + (\gamma_{21}^{+}/\omega_2)]r_1^{(0)2},\\
&\Lambda_{31} = \left(\Gamma_1\Gamma_2 F_1\omega_2/F_2\omega_1\right)^{1/2}, \quad \Lambda_{32} = \Gamma_1\left(\Xi^2-1\right)^{1/2}, \quad \Lambda_{33} = 0.
\end{aligned} \tag{B4}$$

The analysis of the dynamics is simplified near the supercritical Hopf bifurcation point $\Delta_F = -\omega_c$, where the state of self-sustained vibrations emerges. Here $r_1^{(0)}, r_2^{(0)} \ll 1$, as seen from Eq. (B3), whereas the ratio $\zeta^{(0)}$ is not small. Therefore, as a first step, we can set $r_1^{(0)} = 0$ in the expressions in Eq. (B4). This leads to a system of two coupled equations for $\delta\zeta$ and $\delta\phi_+$. The corresponding eigenvalues are

$$\lambda_{1,2} \approx -\left(\Gamma_1+\Gamma_2\right) \pm i\omega_c(\Gamma_2-\Gamma_1)/(\Gamma_2+\Gamma_1). \tag{B5}$$

The real and the imaginary parts of λ_1 and λ_2 are both finite at the bifurcation point, as shown in Figs. 3(e) and 3(f).

The third eigenvalue of the matrix $\hat{\Lambda}$ is small, $|\lambda_3| \ll \Gamma_1, \Gamma_2$, near the bifurcation point. It describes the slow decay of $x_3 \equiv \delta r_1$. The variables x_1 and x_2 follow this decay adiabatically. They can be found from Eq. (B4) by setting $\dot{x}_1 = \dot{x}_2 = 0$. Then both x_1 and x_2 are proportional to $\Lambda_{23} \propto r_1^{(0)2}x_3$. The equation for x_3 then takes the form $\dot{x}_3 = \lambda_3 x_3$, with $\lambda_3 \propto -r_1^{(0)2} \propto \Delta_F + \omega_c$.

APPENDIX C: INCREMENT OF THE PHASE DIFFERENCE

In this appendix, we find the values of the phases ϕ_1, ϕ_2 after the transient process that follows incremental change of the driving-field phase θ_F by $\delta\theta_F$. This can be done by diagonalization of the matrix $\hat{\Lambda}$. We introduce right and left eigenvectors of this matrix, $\mathbf{y}_\nu$ and $\bar{\mathbf{y}}_\mu$,

$$\hat{\Lambda}\mathbf{y}_\nu = \lambda_\nu\mathbf{y}_\nu, \quad \bar{\mathbf{y}}_\nu\hat{\Lambda} = \lambda_\nu\bar{\mathbf{y}}_\nu, \quad \bar{\mathbf{y}}_{\nu'}\cdot\mathbf{y}_\nu = \delta_{\nu\nu'}.$$

We then expand $\mathbf{x}(t)$ in $\mathbf{y}$ and use Eq. (B4) to obtain

$$\mathbf{x}(t) = \sum_\nu C_\nu(t)\mathbf{y}_\nu, \quad C_\nu(t) = \exp(\lambda_\nu t)C_\nu(0),$$
$$C_\nu(0) = \bar{\mathbf{y}}_\nu\cdot\mathbf{x}(0). \tag{C1}$$

To fully describe time evolution of the coupled oscillators in response to a perturbation, and in particular in response to the increment of the phase of the drive θ_F, this equation has to be complemented by the expression for the increment of the phase $\delta\phi_-$. The equation for $\delta\phi_-$ can be obtained by linearization of Eq. (6), which gives

$$\begin{aligned}
\frac{d}{dt}\delta\phi_- &= \mathbf{\Phi}\cdot\mathbf{x}, \quad \Phi_1 = -(\Gamma_1+\Gamma_2)(\Xi^2-1)^{1/2}/\zeta^{(0)}\\
&\quad + 2(\gamma_{12}^{-}/\omega_1)r_1^{(0)2}\zeta^{(0)}, \Phi_2 = \Gamma_1-\Gamma_2,\\
\Phi_3 &= 2[(\gamma_{12}^{-}/\omega_1)\zeta^{(0)2} - (\gamma_{21}^{-}/\omega_2)]r_1^{(0)2}.
\end{aligned} \tag{C2}$$

The solution of Eqs. (C1) and (C2) was used in Fig. 3 to illustrate the evolution of the parameters in time.

For $t \gg t_r$, where $t_r = \max|\mathrm{Re}\,\lambda_\nu|^{-1}$ $(\nu = 1,2,3)$, all components of the vector $\mathbf{x}(t)$ go to zero, and therefore $\delta\phi_+(t) \to \delta\theta_F$. To find the change of ϕ_-, we integrate Eq. (C2) over time, which gives in the limit of long time

$$\delta\phi_-(t) \to -\sum_\nu\left(\bar{\mathbf{y}}_\nu\cdot\mathbf{x}(0)\right)\left(\mathbf{\Phi}\cdot\mathbf{y}_\nu\right)/\lambda_\nu. \tag{C3}$$

For $\mathbf{x}(0) = (0, \delta\theta_F, 0)$ this gives $\delta\phi_-(t) \to C\delta\theta_F$, with

$$C = -\sum_\nu (\bar{\mathbf{y}}_\nu)_2 \left(\mathbf{\Phi} \cdot \mathbf{y}_\nu\right)/\lambda_\nu. \tag{C4}$$

This expression was used in Eq. (9) to find the values approached by the phases ϕ_1 and ϕ_2 after a change of the phase of the drive. We note that, even though two of the three eigenvalues λ_ν are complex, it is clear that C is real.

1. Adiabatic change of the drive frequency

Insight into the value of C can be gained by studying the dynamics of the system for slowly varying frequency of the driving field, where Δ_F slowly increases and then decreases back to its original value, $\Delta_F \to \Delta_F + \delta\Delta_F(t)$. We assume that $\delta\Delta_F(t)$ is small and $|d\delta\Delta_F(t)/dt| \ll |\delta\Delta_F(t)|/t_r$. In this case, as seen from Eq. (5), the equation of motion for the increments $\mathbf{x}$ takes the form

$$\dot{x}_i = \sum_j \Lambda_{ij} x_j - \delta\Delta_F(t)\delta_{i,2}, \quad \mathbf{x}(0) = \mathbf{0}.$$

Changing to variables $\mathbf{y}$, as in Eq. (C1), we obtain for the expansion coefficients C_ν

$$\dot{C}_\nu = \lambda_\nu C_\nu - \delta\Delta_F(t)(\bar{\mathbf{y}}_\nu)_2, \tag{C5}$$

where $(\bar{\mathbf{y}}_\nu)_2$ is the second component of the vector $\bar{\mathbf{y}}_\nu$.

Assuming that $\delta\Delta_F(t)$ varies slowly, we can disregard $\dot{C}_\nu$ in this equation, which gives

$$C_\nu = \lambda_\nu^{-1}(\bar{\mathbf{y}}_\nu)_2\delta\Delta_F(t).$$

After a slow pulse $\delta\Delta_F(t)$, the coefficients C_ν become equal to zero.

We now consider Eq. (6) for $\delta\phi_-$. It has the form

$$\frac{d}{dt}\delta\phi_- = \delta\Delta_F(t)\sum_\nu (\bar{\mathbf{y}}_\nu)_2\left(\mathbf{\Phi}\cdot\mathbf{y}_\nu\right)/\lambda_\nu + \delta\Delta_F(t)\left[1 - 2\frac{d}{d\Delta_F}\delta\omega\right]. \tag{C6}$$

To calculate the derivative of $\delta\omega$ in the adiabatic limit, we use Eq. (B3). As seen from this equation, $\delta\omega$ is linear in Δ_F. Since $\zeta^{(0)}$ is independent of Δ_F, we obtain

$$\frac{d}{d\Delta_F}\delta\omega = \left(\frac{\gamma_{12}}{\omega_1}\zeta^{(0)2} + \frac{3\gamma_{11}}{2\omega_1}\right)\frac{\Gamma_2\omega_2 F_1}{\gamma_{21}^{(+)}\Gamma_2 F_1 + \gamma_{12}^{(+)}\Gamma_1 F_2}. \tag{C7}$$

In the adiabatic limit, the value of ϕ_- does not change. Therefore, the coefficient of $\delta\Delta_F(t)$ in Eq. (C6) is equal to zero. Since the first term on the right-hand side of Eq. (C6) is $-C\delta\Delta_F(t)$, the condition $\dot{\phi}_- = 0$ provides a compact form of the expression for C in terms of $d\delta\omega/d\Delta_F$:

$$C = 1 - 2\frac{d\delta\omega}{d\Delta_F}. \tag{C8}$$

An important consequence is that C is independent of the value of Δ_F itself. Moreover, given that $F_1 \propto F_2$, we see that C is independent of the drive amplitude as well.

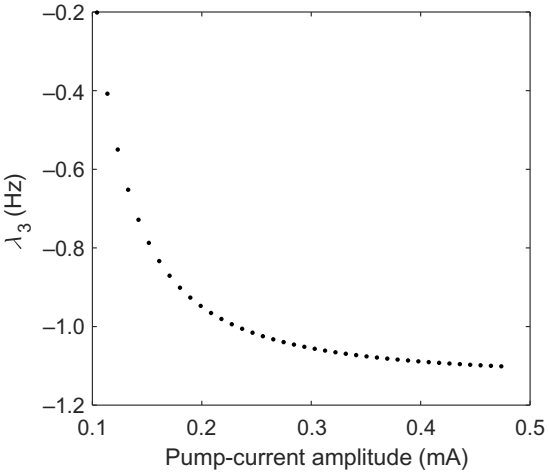

FIG. 7. Dependence of eigenvalue λ_3 of the matrix $\hat{\Lambda}$ in the equation of motion linearized about a stable self-sustained-vibration state on the amplitude of the pump current. The pump-current frequency detuning is 0 Hz.

APPENDIX D: DEPENDENCE OF THE SETTLING TIME ON PUMP CURRENT

The time required for the two modes to settle in response to a step change in θ_F is determined by relaxation time $|\lambda_3^{-1}|$. In terms of stabilizing the frequencies of self-sustained vibrations, it is desirable to have large $|\lambda_3|$ so that the duration of each cycle in the stabilization algorithm can be reduced and θ_F can be updated more frequently to compensate for phase diffusion. Figure 7 shows the dependence of λ_3 on the amplitude of the pump current when the pump detuning frequency is fixed at 0 Hz. Initially, λ_3 becomes more negative rapidly as the pump-current amplitude increases and then levels off. For the data reported in the main text, the pump-current amplitude is chosen to be 189 μA. Further increase in the pump-current amplitude only marginally shortens the relaxation time, but significantly increases the risk of damaging the thin gold layer on the suspended beams.

[1] A. Jenkins, Self-oscillation, Phys. Rep. **525**, 167 (2013).
[2] B. Kim, R. N. Candler, M. A. Hopcroft, M. Agarwal, W.-T. Park, and T. W. Kenny, Frequency stability of wafer-scale

film encapsulated silicon based MEMS resonators, Sens. Actuators, A **136**, 125 (2007).
[3] J. T. M. van Beek and R. Puers, A review of MEMS oscillators for frequency reference and timing applications, J. Micromech. Microeng. **22**, 013001 (2012).
[4] S. Zaliasl, J. C. Salvia, G. C. Hill, L. W. Chen, K. Joo, R. Palwai, N. Arumugam, M. Phadke, S. Mukherjee, H.-C. Lee, C. Grosjean, P. M. Hagelin, S. Pamarti, T. S. Fiez, K. A. A. Makinwa, A. Partridge, and V. Menon, A 3 ppm $1.5 \times 0.8\,\mathrm{mm}^2$ $1.0\,\mu\mathrm{A}$ 32.768 kHz MEMS-based oscillator, IEEE J. Solid-State Circuits **50**, 291 (2015).
[5] M. H. Roshan, S. Zaliasl, K. Joo, K. Souri, R. Palwai, W. Chen, S. Pamarti, J. C. Doll, N. Miller, C. Arft, S. Tabatabaei, C. Sechen, A. Partridge, and V. Menon, in *2016 IEEE International Solid-State Circuits Conference (ISSCC)* (IEEE, San Francisco, CA, USA, 2016), p. 200.
[6] A. Eichler, J. Moser, M. Dykman, and A. Bachtold, Symmetry breaking in a mechanical resonator made from a carbon nanotube, Nat. Commun. **4**, 2843 (2013).
[7] A. N. Cleland and M. L. Roukes, A nanometre-scale mechanical electrometer, Nature **392**, 160 (1998).
[8] D. Rugar, R. Budakian, H. J. Mamin, and B. W. Chui, Single spin detection by magnetic resonance force microscopy, Nature **430**, 329 (2004).
[9] M. S. Hanay, S. Kelber, A. K. Naik, D. Chi, S. Hentz, E. C. Bullard, E. Colinet, L. Duraffourg, and M. L. Roukes, Single-protein nanomechanical mass spectrometry in real time, Nat. Nanotechnol. **7**, 602 (2012).
[10] T. R. Albrecht, P. Grütter, D. Horne, and D. Rugar, Frequency modulation detection using high-Q cantilevers for enhanced force microscope sensitivity, J. Appl. Phys. **69**, 668 (1991).
[11] J. R. Vig and Y. Kim, Noise in microelectromechanical system resonators, IEEE Trans. Ultrason. Ferroelectr. Freq. Control **46**, 1558 (1999).
[12] B. Yurke, D. S. Greywall, A. N. Pargellis, and P. A. Busch, Theory of amplifier-noise evasion in an oscillator employing a nonlinear resonator, Phys. Rev. A **51**, 4211 (1995).
[13] X. L. Feng, C. J. White, A. Hajimiri, and M. L. Roukes, A self-sustaining ultrahigh-frequency nanoelectromechanical oscillator, Nat. Nanotechnol. **3**, 342 (2008).
[14] L. G. Villanueva, R. B. Karabalin, M. H. Matheny, E. Kenig, M. C. Cross, and M. L. Roukes, A nanoscale parametric feedback oscillator, Nano Lett. **11**, 5054 (2011).
[15] E. Kenig, M. C. Cross, L. G. Villanueva, R. B. Karabalin, M. H. Matheny, R. Lifshitz, and M. L. Roukes, Optimal operating points of oscillators using nonlinear resonators, Phys. Rev. E **86**, 056207 (2012).
[16] D. Antonio, D. H. Zanette, and D. López, Frequency stabilization in nonlinear micromechanical oscillators, Nat. Commun. **3**, 806 (2012).
[17] C. Chen, D. H. Zanette, J. R. Guest, D. A. Czaplewski, and D. López, Self-sustained micromechanical oscillator with linear feedback, Phys. Rev. Lett. **117**, 017203 (2016).
[18] L. Huang, S. M. Soskin, I. A. Khovanov, R. Mannella, K. Ninios, and H. B. Chan, Frequency stabilization and noise-induced spectral narrowing in resonators with zero dispersion, Nat. Commun. **10**, 3930 (2019).
[19] M. Defoort, S. Hentz, S. W. Shaw, and O. Shoshani, Amplitude stabilization in a synchronized nonlinear nanomechanical oscillator, Commun. Phys. **5**, 93 (2022).
[20] A. Velikovich, G. Golubev, V. Golubchenko, and D. Luchinsky, Tristability and self-oscillations in a double resonator system, Opt. Commun. **80**, 444 (1991).
[21] M. Zalalutdinov, A. Zehnder, A. Olkhovets, S. Turner, L. Sekaric, B. Ilic, D. Czaplewski, J. M. Parpia, and H. G. Craighead, Autoparametric optical drive for micromechanical oscillators, Appl. Phys. Lett. **79**, 695 (2001).
[22] R. A. Barton, I. R. Storch, V. P. Adiga, R. Sakakibara, B. R. Cipriany, B. Ilic, S. P. Wang, P. Ong, P. L. McEuen, J. M. Parpia, and H. G. Craighead, Photothermal self-oscillation and laser cooling of graphene optomechanical systems, Nano Lett. **12**, 4681 (2012).
[23] R. De Alba, T. S. Abhilash, R. H. Rand, H. G. Craighead, and J. M. Parpia, Low-power photothermal self-oscillation of bimetallic nanowires, Nano Lett. **17**, 3995 (2017).
[24] B. J. Roxworthy and V. A. Aksyuk, Electrically tunable plasmomechanical oscillators for localized modulation, transduction, and amplification, Optica **5**, 71 (2018).
[25] J. S. Ochs, D. K. J. Boneß, G. Rastelli, M. Seitner, W. Belzig, M. I. Dykman, and E. M. Weig, Frequency comb from a single driven nonlinear nanomechanical mode, Phys. Rev. X **12**, 041019 (2022).
[26] S. Etaki, F. Konschelle, Ya. M. Blanter, H. Yamaguchi, and H. S. J. van der Zant, Self-sustained oscillations of a torsional SQUID resonator induced by Lorentz-force back-action, Nat. Commun. **4**, 1803 (2013).
[27] S. Schmid, L. G. Villanueva, and M. L. Roukes, *Fundamentals of Nanomechanical Resonators* (Springer, Switzerland, 2016).
[28] A. Demir and M. S. Hanay, Fundamental sensitivity limitations of nanomechanical resonant sensors due to thermomechanical noise, IEEE Sens. J. **20**, 1947 (2020).
[29] A. Bachtold, J. Moser, and M. I. Dykman, Mesoscopic physics of nanomechanical systems, Rev. Mod. Phys. **94**, 045005 (2022).
[30] S. M. Rytov, Fluctuations in oscillating systems of the Thompson type 1, Sov. Phys. JETP-USSR **2**, 217 (1956).
[31] S. M. Rytov, Fluctuations in oscillating systems of the Thompson type 2, Sov. Phys. JETP-USSR **2**, 225 (1956).
[32] E. Rubiola, *Phase Noise and Frequency Stability in Oscillators* (Cambridge University Press, Cambridge, 2009).
[33] N. J. Miller, S. W. Shaw, and M. I. Dykman, Suppressing frequency fluctuations of self-sustained vibrations in underdamped nonlinear resonators, Phys. Rev. Appl. **15**, 014024 (2021).
[34] C. Zhao, G. Sobreviela, M. Pandit, S. Du, X. Zou, and A. Seshia, Experimental observation of noise reduction in weakly coupled nonlinear MEMS resonators, J. Microelectromech. Syst. **26**, 1196 (2017).
[35] D. S. Greywall, B. Yurke, P. A. Busch, A. N. Pargellis, and R. L. Willett, Evading amplifier noise in nonlinear oscillators, Phys. Rev. Lett. **72**, 2992 (1994).
[36] E. Kenig, M. C. Cross, J. Moehlis, and K. Wiesenfeld, Phase noise of oscillators with unsaturated amplifiers, Phys. Rev. E **88**, 062922 (2013).
[37] L. G. Villanueva, E. Kenig, R. B. Karabalin, M. H. Matheny, R. Lifshitz, M. C. Cross, and M. L. Roukes,

Surpassing fundamental limits of oscillators using nonlinear resonators, Phys. Rev. Lett. **110**, 177208 (2013).
[38] E. Kenig, M. C. Cross, R. Lifshitz, R. B. Karabalin, L. G. Villanueva, M. H. Matheny, and M. L. Roukes, Passive phase noise cancellation scheme, Phys. Rev. Lett. **108**, 264102 (2012).
[39] I. L. Berstein, On fluctuations in the neighborhood of periodic motion of an auto-oscillating system, Sov. Acad. Sci. Dokl. **20**, 11 (1938).
[40] H. Haken, Theory of intensity and phase fluctuations of a homogeneously broadened laser, Z. Phys. **190**, 327 (1966).
[41] M. Lax, Classical noise v. noise in self sustained oscillators, Phys. Rev. **160**, 290 (1967).
[42] D. K. Agrawal and A. A. Seshia, An analytical formulation for phase noise in MEMS oscillators, IEEE Trans. Ultrason. Ferroelectr. Freq. Control **61**, 1938 (2014).
[43] F. Sun, X. Dong, J. Zou, M. I. Dykman, and H. B. Chan, Correlated anomalous phase diffusion of coupled phononic modes in a sideband-driven resonator, Nat. Commun. **7**, 12694 (2016).
[44] A. Demir, A. Mehrotra, and J. Roychowdhury, Phase noise in oscillators: A unifying theory and numerical methods for characterization, IEEE Trans. Circuits Syst. Fundam. Theory Appl. **47**, 655 (2000).
[45] I. Mahboob, K. Nishiguchi, H. Okamoto, and H. Yamaguchi, Phonon-cavity electromechanics, Nat. Phys. **8**, 387 (2012).
[46] T. J. Kippenberg and K. J. Vahala, Cavity optomechanics: Back-action at the mesoscale, Science **321**, 1172 (2008).
[47] M. Aspelmeyer, T. J. Kippenberg, and F. Marquardt, Cavity optomechanics, Rev. Mod. Phys. **86**, 1391 (2014).
[48] M. Dykman, Heating and cooling of local and quasilocal vibrations by a nonresonance field, Sov. Phys. Solid State **20**, 1306 (1978).
[49] F. Marquardt, J. G. E. Harris, and S. M. Girvin, Dynamical multistability induced by radiation pressure in high-finesse micromechanical optical cavities, Phys. Rev. Lett. **96**, 103901 (2006).
[50] T. J. Kippenberg, H. Rokhsari, T. Carmon, A. Scherer, and K. J. Vahala, Analysis of radiation-pressure induced mechanical oscillation of an optical microcavity, Phys. Rev. Lett. **95**, 033901 (2005).
[51] T. Carmon, H. Rokhsari, L. Yang, T. J. Kippenberg, and K. J. Vahala, Temporal behavior of radiation-pressure-induced vibrations of an optical microcavity phonon mode, Phys. Rev. Lett. **94**, 223902 (2005).
[52] C. Metzger, M. Ludwig, C. Neuenhahn, A. Ortlieb, I. Favero, K. Karrai, and F. Marquardt, Self-induced oscillations in an optomechanical system driven by bolometric backaction, Phys. Rev. Lett. **101**, 133903 (2008).
[53] M. Bagheri, M. Poot, M. Li, W. P. H. Pernice, and H. X. Tang, Dynamic manipulation of nanomechanical resonators in the high-amplitude regime and non-volatile mechanical memory operation, Nat. Nanotechnol. **6**, 726 (2011).
[54] T. Faust, P. Krenn, S. Manus, J. Kotthaus, and E. Weig, Microwave cavity-enhanced transduction for plug and play nanomechanics at room temperature, Nat. Commun. **3**, 728 (2012).
[55] F. M. Buters, H. J. Eerkens, K. Heeck, M. J. Weaver, B. Pepper, S. de Man, and D. Bouwmeester, Experimental exploration of the optomechanical attractor diagram and its dynamics, Phys. Rev. A **92**, 013811 (2015).